AD_____

Award Number: W81XWH-04-1-0239

TITLE: Early Detection of Breast Cancer by Fluorescence Molecular Tomography

PRINCIPAL INVESTIGATOR: Vasilis Ntziachristos, Ph.D.
Stephen D. Windsor

CONTRACTING ORGANIZATION: The General Hospital Corporation
Massachusetts General Hospital
Boston, MA 02114

REPORT DATE: July 2005

TYPE OF REPORT: Annual

PREPARED FOR: U.S. Army Medical Research and Materiel Command
Fort Detrick, Maryland 21702-5012

REPORT DOCUMENTATION PAGE

Form Approved
OMB No. 0704-0188

1. REPORT DATE *(DD-MM-YYYY)*	2. REPORT TYPE	3. DATES COVERED *(From - To)*
01-07-2005	Annual	1 Jul 04 – 30 Jun 05

4. TITLE AND SUBTITLE
Early Detection of Breast Cancer by Fluorescence Molecular Tomography

5a. CONTRACT NUMBER

5b. GRANT NUMBER
W81XWH-04-1-0239

5c. PROGRAM ELEMENT NUMBER

6. AUTHOR(S)
Vasilis Ntziachristos, Ph.D.
Stephen D. Windsor

E-Mail: vasilis@helix.mgh.harvard.edu

5d. PROJECT NUMBER

5e. TASK NUMBER

5f. WORK UNIT NUMBER

7. PERFORMING ORGANIZATION NAME(S) AND ADDRESS(ES)

The General Hospital Corporation
Massachusetts General Hospital
Boston, MA 02114

8. PERFORMING ORGANIZATION REPORT NUMBER

9. SPONSORING / MONITORING AGENCY NAME(S) AND ADDRESS(ES)
U.S. Army Medical Research and Materiel Command
Fort Detrick, Maryland 21702-5012

10. SPONSOR/MONITOR'S ACRONYM(S)

11. SPONSOR/MONITOR'S REPORT NUMBER(S)

12. DISTRIBUTION / AVAILABILITY STATEMENT
Approved for Public Release; Distribution Unlimited

13. SUPPLEMENTARY NOTES

14. ABSTRACT

Early detection of breast tumors continues to be a significant diagnostic challenge and thus remains the focus of attention of a number of medical research groups. Molecular targeting approaches have tremendous potential for early-detection because they rely on elucidation of abnormal gene-expression, rather than on discovery of retarded anatomical changes inflicted by growing tumors upon their microenvironment. Originally, we proposed an investigation of whether highly-sensitive fluorescence molecular tomography (FMT) could be used to detect breast cancer at its earliest and smallest stages via the detection of injected, protease-activatable molecular probes. We enter year 2 with the year 1 goals fully achieved, having completed construction of the proposed FMT imaging system and having optimized the system using phantoms. Furthermore, we have made significant progress toward accomplishing the goals for year 2 by beginning the in-vivo early detection and screening studies ahead of schedule.

15. SUBJECT TERMS
Molecular imaging, fluorescence, tomography, early detection, specificity, breast cancer

16. SECURITY CLASSIFICATION OF:			17. LIMITATION OF ABSTRACT	18. NUMBER OF PAGES	19a. NAME OF RESPONSIBLE PERSON
a. REPORT	b. ABSTRACT	c. THIS PAGE			USAMRMC
U	U	U	UU	31	19b. TELEPHONE NUMBER *(include area code)*

Table of Contents

Introduction

Breast cancer is the second most common female malignancy in the United States. The ability to detect malignancies in their earliest stages is of tremendous importance. Early detection has been shown to increase likelihood of survival [1, 2] and to reduce the risk of disease recurrence [3 – 6]. However, early detection continues to be a significant diagnostic challenge and thus remains the focus of attention of a number of medical research groups.

Well-established detection techniques, most notably mammography, remain limited in their sensitivity to small-volume disease. Though mammography has been of great importance for detection of breast malignancies, many tumors have evaded detection by this method largely due to its limited contrast. The technique is particularly hampered by background interference such as increased tissue density or scarring from prior surgery. Functional imaging, which includes Magnetic Resonance Imaging (MRI) and Positron Emission Tomography (PET), has been used as a compliment to anatomical imaging and has shown significant potential to image functional characteristics of tumors [7]. However, the high cost and complex operational logistics of these modalities may limit their practicality for use in large-scale screening studies.

An additional parameter that plays a vital role in breast cancer detection is the ability to detect specific disease signatures based on the molecular profile of the disease. Molecular imaging, i.e., imaging of cellular and sub-cellular processes that are associated with molecular onset and evolution of disease, can lead to increased sensitivity and specificity and can improve the overall performance of a diagnostic study. Improved specificity, based on the detection of molecular profiles, can lead to the overall reduction in unnecessary biopsies, which are associated with increased healthcare costs and patient distress, and thus can lead to personalized medicine. It is foreseen that such methods will help optimize therapeutic strategies and will enable the effects of treatment to be more closely followed in time scales of hours or days instead of the longer timeframe of weeks or months that is the current standard for on anatomical imaging methods. Some of our recent review articles [8, 9] provide more detailed discussions of molecular imaging in general, and one of our recent studies [10] demonstrates the ability of optical imaging to monitor disease behavior.

Optical methods have emerged as economic, safe, and effective alternatives for functional imaging. Diffuse Optical Tomography (DOT) has been developed for imaging of breast cancers because of its ability to non-invasively quantify oxy- and deoxy-hemoglobin concentrations, which can be used to characterized angiogenesis and hypoxia [11-15]. In addition, DOT has been used in combination with MRI to detect tumors based on the extrinsically-administered contrast agent Indocyanine Green (ICG) that marks angiogenesis and permeability. However, these markers, though they enable DOT to effectively image well-developed tumors, are not ideal for detection of the earliest stages of disease. Consequently, while DOT may certainly be a useful tool for evaluating larger tumors, a more effective optical modality is needed for early detection.

Fluorescence Molecular Tomography (FMT) is a relatively new optical tomographic imaging approach that capitalizes on the strengths of molecular imaging. It bases detection on specific molecular signatures, using highly targeted fluorescent probes, rather than on anatomical or functional changes within tumor microenvironments. This approach yields a shift in the radiological paradigm that has traditionally focused on anatomy and physiology [16]. Unlike DOT, FMT can three-dimensionally resolve protein expression, protease activity, receptor regulation, and similar molecular markers that play vital roles in carcinogenesis. It has been demonstrated in-vivo that NIR photons can penetrate more than 12 centimeters into the breast, and that fluorochromes accumulating in small tumors are detectable through the human breast [17]. We have previously shown that FMT is capable of resolving phantoms placed less than 1 mm apart [18], and the sensitivity of this technology has been predicted to be adequate for detection of human breast lesions smaller than 5 mm [19]. More recently it has been shown that the technique can visualize apoptosis as a response to treatment [10]. Furthermore, because non-ionizing radiation is used, the technology allows for repeated imaging for screening or monitoring of disease. FMT thus holds great promise for early detection of breast malignancies.

At the time of our grant proposal, several elegant targeted fluorescent probes had already been developed [20-22] for use with optical methods such as FMT. Among the most notable of these were the so-called "smart" probes (also termed "activatable probes"), which are optically silent until they interact with a specific enzyme, such as a protease, which then activates the probe, converting it to a brightly fluorescent state [20]. These probes are powerful not only because of their specificity for cancer-associated enzymatic activity, but also because they significantly minimize background levels and exhibit several-fold amplification of fluorescence upon activation, enabling dramatic improvements in signal-to-noise contrast. Because activatable probes fluorescence only in the presence of specific tumor phenotypes, they can easily be localized and quantified against a virtually "dark" background, allowing for highly sensitive and specific detection.

Our proposal described using a smart probe that is activated by major cathepsins, which are members of the cysteine family of proteases and play a central role in tumorigenesis and matrix invasion [23-26]. For example, it has been demonstrated that high levels of cathepsin B expression correlates positively with aggressive behavior and progression of human tumors and negatively with patient survival [23]. We therefore chose to evaluate the performance of this probe for imaging breast cancer development and progression.

Until the study was supported by this grant, in-vivo imaging of such probes were limited to basic feasibility studies, generally involving imaging of xenographic implants in nude mice. Generally, it was unknown how early in disease progression such probes could be used to reliably detect malignancies, as the in-vivo sensitivity limits of FMT have not been rigorously explored. The goals of our proposal were primarily (1) to develop and optimize optical technology for highly

sensitive detection; and (2) to evaluate the early-detection limits of FMT by conducting a blind screening study of transgenic mice that develop spontaneous tumors of the mammary fat pad, closely mimicking the natural development and progression of human breast cancer. We proposed developing imaging tools designed to systematically reduce background noise levels and to improve fluorochrome localization and quantification. The study was designed to investigate screening efficacy and to predict sensitivity limits of human breast cancer.

The hypothesis of this proposal is that highly sensitive fluorescence imaging (tomosynthesis) of molecular contrast will enable earlier detection of breast tumors based on signals associated with tumor growth and matrix invasion. We predicted that this technology could achieve high detection specificity.

Our study had three major goals:

Aim 1. *To develop appropriate photon illumination and detection strategies and reconstruction methods for highly sensitive fluorescence detection and quantification.*

Aim 2. *To utilize optimal photon technology from Aim 1 to study in-vivo detection of spontaneous disease in transgenic mice and to follow local disease progression and distant metastases.*

Aim 3. *To translate the animal study findings into clinically-relevant detection schemes.*

The first of these aims was designed to find an optimal illumination technology and processing method in order to obtain the highest detection sensitivity of fluorochromes in tissues. We proposed investigating limited angle projections versus multi-angle illumination, planar illumination, and transillumination schemes.

The second aim focused on the clinical relevance of FMT. We proposed a screening study involving transgenic mice that spontaneously develop breast tumors. Our interest was and continues to be primarily (1) to characterize detection capacity as a function of disease progression and tumor growth; and (2) to quantify fluorescence concentration in-vivo and determine whether it correlates with tumor expression profiles. This screening study would enable us to establish early-detection limits.

The third aim was to translate the copious data acquired from exploring the first two aims into an evaluation of the clinical feasibility of FMT for early-detection of breast cancer.

In the grant proposal we presented a timeline for accomplishing our primary aims for years 1 – 3 of the study (Table 1).

Table.1 Overview of aims and time line

	Year 01	Year 02	Year 03
Aim 1: Method Development & Optimization			
• Construction of 4-mode imaging chamber	X		
• Developing imaging algorithms	X		
• Optimizing imaging parameters with phantoms	X		
• Optimize imaging parameters with orthotopic mouse model(s)		X	
Aim 2: In vivo Screening study			
• Establish appropriate transgenic mouse model(s)	X		
• Breed and screen mice for early detection of tumors		X	X
• Study local and distant disease progression.		X	X
Aim 3: Clinical translation			
• Construction of breast-like phantoms		X	X
• Experiments with phantoms			X
• Simulations			X

To date, we have not only met, but also exceeded the goals for year 1, and we have also made significant progress in reaching the goals for year 2. The following sections provided a detailed evaluation of our progress.

Body

We have completed all of the goals set for year 1, which encompasses all of Aim 1 and a small portion of Aim 2. Furthermore, we have made significant progress towards achieving Aim 2 and thus have a strong head-start in completing the goals for year 2. The following is a detailed description of accomplishments and reported outcomes achieved over the past year:

Aim 1. ***To develop appropriate photon illumination and detection strategies and reconstruction methods for highly sensitive fluorescence detection and quantification.***

A1.1: Construction of an integrated illumination/detection small animal imaging system.

We constructed a 4-mode imaging chamber, a schematic of which is presented in Figure 1. Photographs of the system are shown in Figure 2. This system is based on a previously-reported scanner [18]. Illumination is provided by either a 672 nm wavelength or a 748 nm wavelength cw laser (a) routed to a two-channel optical switch (b). One output of this switch connects to an illumination branch (f) for *reflectance imaging* (g), while the other output connects a source fiber (c) to a 1x46 optical switch (d) which establishes all the other three imaging modes. The 1x46 switch multiplexes the single light input (c) to 46 output fibers (e), which couple the laser light from the switch to the animal chamber (h). The 46 fibers are inserted through the backside of the animal chamber, abutting the inner back wall, and are arranged equidistantly in a hexagonal mesh. The chamber is identical to ones that have been described previously (Graves et al 2003).

Furthermore, since the grant proposal we have constructed a rotational stage and mouse holder (Figure 2, right) that may be inserted into the chamber to achieve complete projection (360) geometry. A low noise, 512x512 element cooled CCD camera (k) collects photons that pass through appropriate bandpass filters (i). Data is then processed using a 3.20 GHz Pentium 4 personal computer with 2 GB of RAM running Windows XP (n). The system accommodates all four illumination schemes that were described in the grant proposal, namely *reflectance imaging, transillumination, tomosynthesis,* and *tomography.* These illumination schemes are also shown in Figure 3.

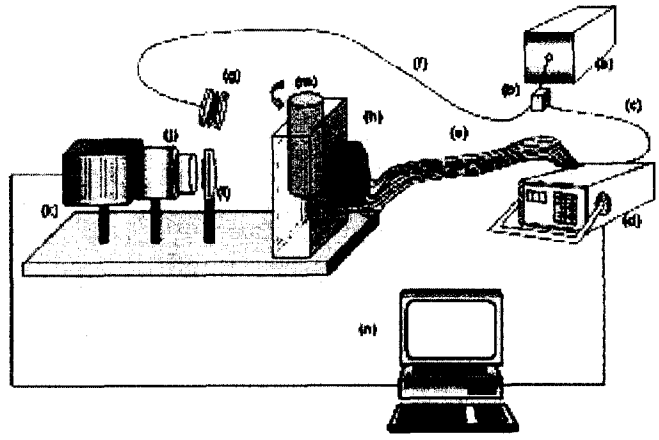

Figure 1: FMT imaging system.

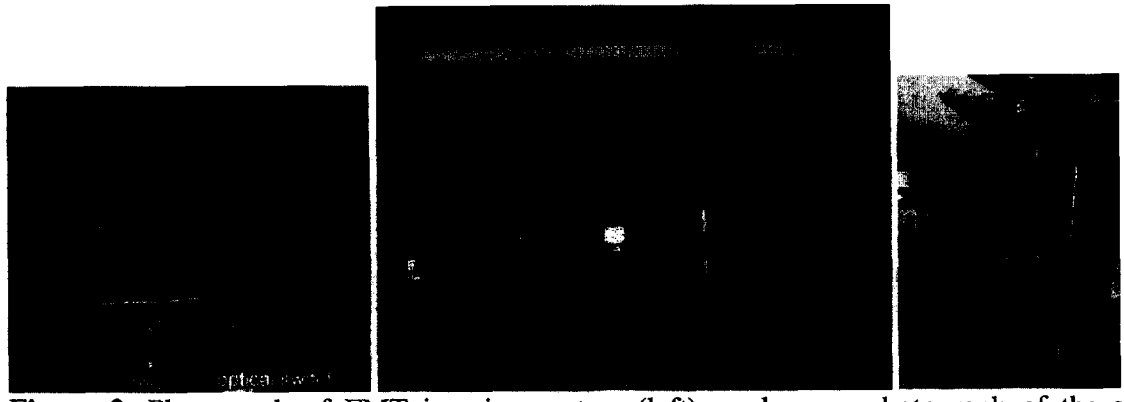

Figure 2: Photograph of FMT imaging system (left), a close-up photograph of the system (middle), and a photograph of the rotational stage with a mouse in place in the holder (right), which can be placed into the imaging chamber for complete projection (360^0) geometry.

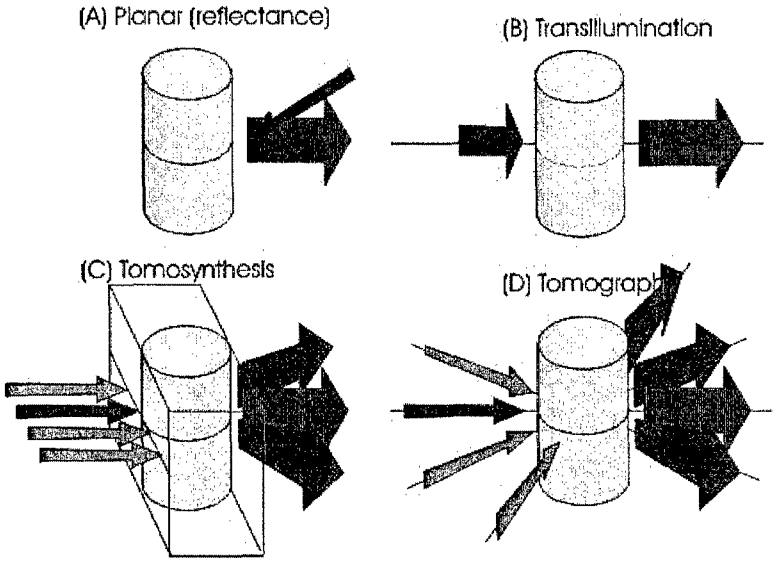

Figure 3:. Schematics of the 4 modes of imaging

Reflectance Imaging

The illumination branch (Figure 1, f, g; Figure 3, middle) illuminates the animal through the chamber window, and reflected intrinsic or fluorescence photons are recorded on the CCD

Figure 4: Intrinsic (left) and fluorescence (right) reflectance images of a mouse with subcutaneous tumors (red arrows in right image). The liver is indicated with a white arrow. The mouse was injected with 2 nmol of a cathepsin-activatable probe 24 hours prior to imaging.

camera using band-pass filters. Figure 4 presents intrinsic and fluorescence reflectance images of a mouse with two subdermal tumors within the mammary fat pads, the result of subcutaneous implantation of 3 x 10^6 HT-1080 cells into each tumor site. Twenty-four hours prior to imaging, the mouse was injected with 2 nmol of a cathepsin-activatable NIR probe. The intrinsic image is useful for anatomical coregistration of the fluorescence image, which clearly shows two tumors as well as the liver, which is known to activate the probe.

Transillumination.

Each of the 46 source fibers directed toward the back of the imaging chamber (Figure 1, e) is sequentially switched on, the transmitted pattern is filtered with appropriate intrinsic or fluorescence band pass filters, and photons are recorded on the CCD camera. The resulting images are added together to create a composite image, which is geometrically similar to an X-ray mammogram. The fluorescence composite image may also be divided by the intrinsic composite image to generate a normalized image, which significantly reduces sensitivity to background heterogeneity and thus provides a more accurate image. Another effective approach is to normalize each of the 46 fluorescence images individually by their corresponding intrinsic images prior to summation (Figure 5). Figure 6 demonstrates an example of transillumination imaging on a mouse with a mammary tumor implanted in the right side of the animal. The

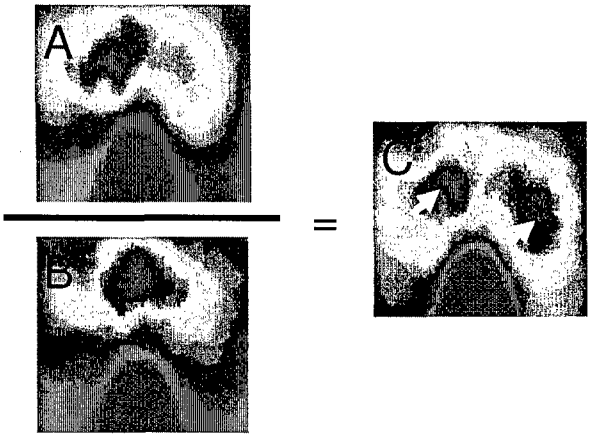

Figure 5: Construction of a transillumination composite image of a mouse with subcutaneous mammary tumors; the images are of a region of interest chosen to encapsulate the tumors. The mouse was injected with a cathepsin-activatable NIR probe 24-hours prior to imaging. Fluorescence transillumination images (A) were divided by corresponding intrinsic transillumination images (B). Low thresholds were applied to the images prior to normalization to reduce background noise. The individually-normalized images were added to create a composite image (C) that provides a more accurate localization of fluorescence signal. Arrowheads indicate tumor locations.

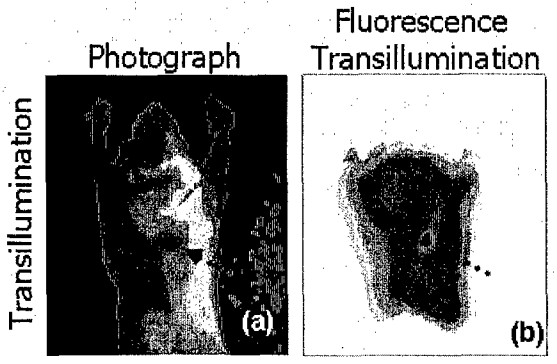

Figure 6: Transillumination imaging of breast tumors. (a) Photograph of the animal. The arrow indicates the position of the tumor. (b) Inverted transillumination image after data normalization reveals higher fluorescence from the tumor (darker indicates higher signal), which is associated with up-regulation of cathepsins.

animal was injected with a protease activated probe 24-hours prior to imaging. Generally, transillumination imaging is better suited for volumetric measurements compared to reflectance imaging because the whole animal volume is probed. This is because light is passing through the animal and, therefore, excites all fluorescence present in its path.

Tomosynthesis.

We had made significant progress with implementing limited angle projection FMT, the equivalent of FMT tomosynthesis. For this approach data is gathered in the same manner as in the transillumination approach; however, unlike that approach, tomosynthesis involves applying algorithms to the data that solve a volume integral equation relating spatially-distributed fluorochrome concentrations (in physical units) to the transillumination measurements. Inversion is performed using an algebraic reconstruction technique with convergence assumed after 20 iterations, as empirically-determined to yield optimal imaging performed based on phantom measurements. This process yields a three-dimensional "map" of fluorochromes concentration that is subsequently sliced for viewing (Figure 7).

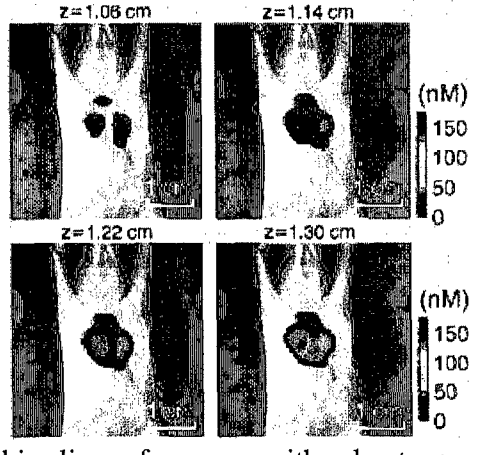

Figure 7: Tomographic slices of a mouse with subcutaneous tumors.

Tomography.

To achieve superior imaging performance it is important to illuminate using a large number of projections and detect signal around the animal, similarly to other tomographic techniques such as X-ray CT, PET or SPECT. For this reason we have implemented the rotational device (Figure 1, m) which rotates the object of interest in front of the illumination path and CCD camera to implement a number of projections. The system attains rotational accuracy of better than 0.5 degree, but generally a fewer number of projections is used (typically varying from 72 to 18). Figure 8 shows an example of imaging, in this case also utilizing photon pulses and time-gated detection. In this example a solid phantom was utilized, made of polyester resin in which TiO2 particles and India Ink were added to yield absorption and scattering. The phantom was cut in the cross-sectional shape of a rectangle and a square as shown in Figure 8a and was immersed in a 1% intralipid solution which similarly also contained India Ink to yield absorption. The optical properties of the intralipid-ink solution were (μ_a=0.1 cm^{-1} μ_s'= 7 cm^{-1}) whereas the solid phantom demonstrated 8x this background attenuation.

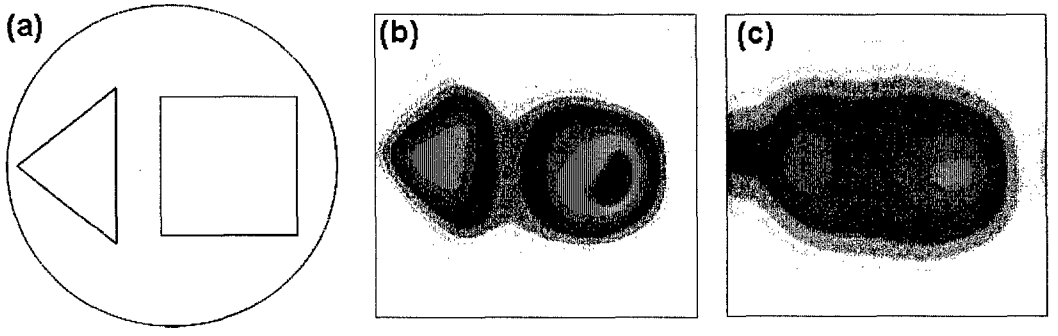

Figure 8: Complete projection tomography imaging here in a diffusive phantom of a triangle and a square. (a) Schematic of the arrangement of the phantom. (b) 360^0 projection reconstructed image using early photons. (c) 360^0 projection reconstructed image using CW.

The reconstructed images are shown in Figures 8b and c respectively. Figure 8b demonstrates the ability of early photons to reconstruct correctly the position and shape of the phantoms. Figure 8c, which is based on CW data also reconstructs the position of the phantoms but cannot reconstruct shape due to the diffusive nature of the phantom. However, although contrast is reduced, the position and size of the phantoms is also reconstructed. In year 2 we will continue optimizing the parameters for reconstruction of CW data based on complete projection tomography data and expect superior reconstruction to be achieved.

A1.2: Development of imaging software

In this first year we have achieved the following advancements in terms of imaging software:

1. Developed algorithms for transillumination imaging using appropriate normalized techniques to improve contrast and robustness (1 publication in press to appear in J. of Biomedical Optics)
2. Developed advanced background fluorescence techniques based on physical models and improve on tomographic performance and contrast (1 publication in preparation)
3. Evaluated algorithms for robust imaging in highly heterogeneous backgrounds as appropriate for in-vivo imaging (One publication in press to appear in IEEE transaction on Medical Imaging)
4. Adapted algorithms already developed for tomosynthesis to complete-projection imaging.

A1.3: Phantom studies

We performed several phantom studies to evaluate the different algorithms developed and assess the overall performance of the method. In particular we constructed highly heterogeneous phantoms using combinations of solid and liquid diffusive media and investigated the performance of the methods with a varying degree of heterogeneity (for examples see appendix). In addition we streamlined the developed of resin phantoms (Figure 9), of different optical properties that can simulate tissues of different optical properties (for example varying optical properties in the breast due to aging).. We have further examined the effects of background fluorescence in homogeneous and heterogeneous phantoms (paper in preparation). We further confirmed previous studies [19, 27] with liquid phantoms attaining the optical properties of the human breast that detection sensitivity is of the order of 10 nM (volume: 200 μl) of fluorescence dye (Cy5.5 ex wvl: 672 nm, max em wvl 690 nm; 5 sec exposure per source) at a phantom with the optical properties of the breast at 2 cm width. In accordance to our time-plan, in year 2 we will build breast like phantoms and test sensitivity limits with phantoms that bear geometrical resemblance to the breast to further evaluate these figures.

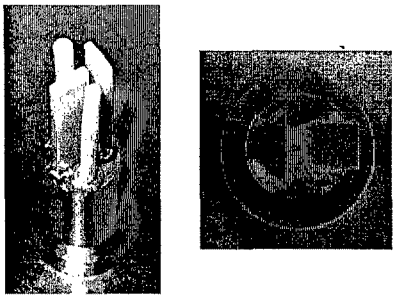

Figure 9: Two photographs of resin phantoms of different shapes and varying degrees of absorbance and fluorescence.

A1.4: Evaluation of imaging practices.

We further undertook studies to compare the performance of planar and tomographic methods to quantify fluorochromes as a function of depth and optical properties. Here we summarize some of the findings, although more details can be found in the appendix.

The first study compared planar imaging and tomosynthesis (tomographic) performance in a side by side comparison. Shown in Figure10a is imaging of two ~1.5mm diameter fluorescent tubes (500nM Cy5.5, 3mm apart) immersed at different depths in a water solution of intralipid and India ink simulating the optical properties of tissue. Both modalities resolve the tubes when placed superficially although FMT offers better resolution. However, detection becomes highly

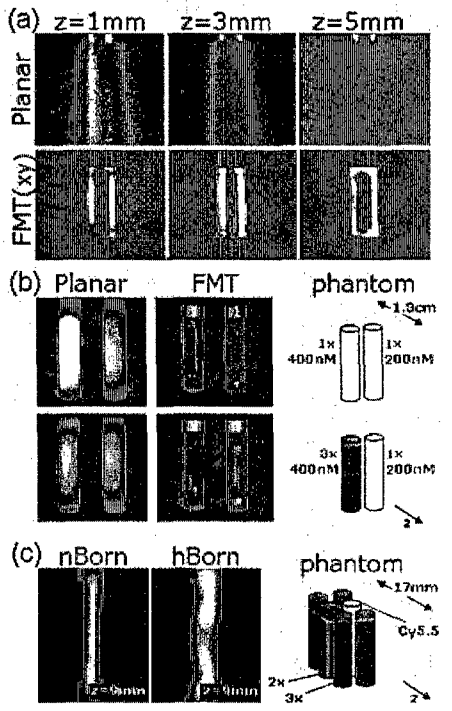

Figure 10: Side-by-side comparison of planar and tomographic imaging (a) as a function pf depth, (b) as a function of varying local optical properties, and (c) as a function of heterogeneity. In all cases tomosynthesis (tomography) is shown superior to planar imaging.

challenging as a function of depth for planar imaging with the tubes barely visible even 3mm deep. Depth sensitivity highly depends on the size and strength of fluorochrome, but the images contrast the superior ability of tomography to look deeper in diffuse media and with higher resolution, using in this case identical hardware to the one used for planar imaging. The color

images are reconstructed slices obtained at different depths and superimposed on gray scale photographs of the tubes for visualization purposes. Similar results are obtained in comparisons of transillumination and tomography, although transillumination can still record objects deeper than in planar imaging. Similarly, the ability to image fluorochromes with varying background optical properties is showcased in Figure 10b, which depicts planar and reconstructed images of two fluorescent tubes, the left tube containing double the amount of Cy5.5 in the right tube (400nM vs. 200nM). The tubes are immersed in the same diffuse fluid as in (a). Both techniques accurately resolve the 2:1 relation in fluorochrome concentration between left and right tubes when background absorption is the same in both tubes (top row). However when India Ink is added in the left tube to simulate a three-fold increase in vascularization (absorption), planar performance is significantly reduced, erroneously reporting a 1:1 Cy5.5 concentration in the two tubes (bottom row). This is because the added ink absorbs more fluorescent photons. In contrast tomography can correct for these phenomena and demonstrates more robust performance reporting 1.8:1 relation in this case. Finally, Figure 10c demonstrates the capacity of tomography to resolve a single fluorescent tube in the middle of a highly diffusive medium when it is asymmetrically surrounded by 5 strong absorbers of 2x and 3x the background absorption and of comparable sizes. This result demonstrates the robustness of tomography to image highly heterogeneous media, an ability that is mainly due to the data normalization techniques (image labeled nborn) employed tomographically. Absence of normalization results in distorted tomographic imaging performance (shown in the image labeled nBorn). Both images are slices from a three dimensional reconstruction obtained at 9mm depth. Planar imaging could not detect the presence of a fluorochrome in this highly absorbing and heterogeneous background.

Overall, these findings exemplify that planar imaging should be used with caution. Signal intensity relates linearly to fluorochrome concentration but non-linearly to depth, size and optical properties and is further complicated by the high scattering nature of tissue. Tomosynthesis and tomography have the potential to improve on these limitations and to offer more robust and accurate imaging.

Aim 2. ***To utilize the optimal photon technology found in Aim1 to study in vivo detection of spontaneous disease in transgenic mice and to follow local disease progression, distant metastases and treatment response.***

As stated in the grant proposal, we selected a transgenic mouse model (c-neu oncogene; strain name FVB/N-TgN(MMTVneu)202Mul, Jackson Laboratory, Bar Harbor, Maine) that accurately mimics known genetic alterations seen in human breast cancer. In this model the mouse mammary virus tumor (MMTV) promoter directs expression of the c-neu oncogene to the mammary fat pads. The model was originally reported to develop mammary tumors in 50% of females by 89 days, but ultimately there is 90% penetrance by 5-6 months. The model is of high biological relevance because the Her-2/neu gene is over-expressed in over 90% of human breast cancers.

A2.3: Imaging studies

Thus far 16 mice have resulting from breeding and have completed screening. Currently an additional 16 mice are approaching the age of tumor onset and will soon be enter imaging studies. Therefore, we foresee successful completion of imaging studies involving a total of 60 transgenic mice (40 experimental mice, 10 control mice, and 10 mice for purposes of parameter optimizations) within the allotted time as originally stated in the grant proposal.

As stated previously in the grant proposal, the purpose of the imaging study is to explore the early-detection and disease-monitoring abilities of FMT. Figure 11 presents results from a mouse with a developing tumor and showcases the ability of the system to follow tumor development over time. Furthermore, it was found that fluorochrome concentration, as calculated by FMT, increased monotonically with tumor diameter (Figure 12), an expected and important result, as it is predicted that probe will accumulate and activate selectively within tumors and that, consequently, larger tumors should display higher concentration of activated probe.

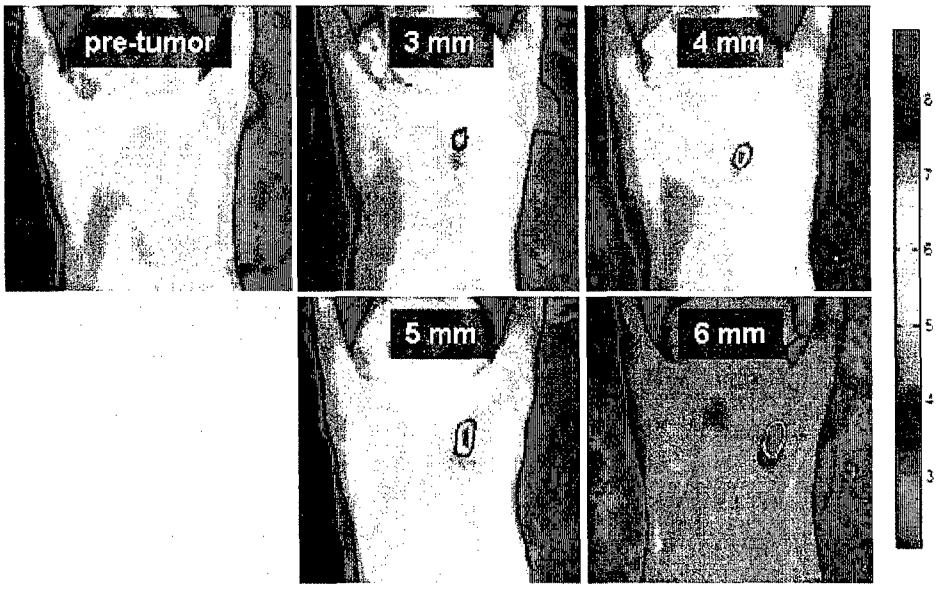

Figure 11: A mouse imaged prior to visible manifestation of tumors and subsequently imaged on a weekly basis to follow tumor growth from 3 mm to 6 mm in diameter. The mouse was injected via tail-vein with 2 nmol of a cathepsin-activatable NIR probe 24-hours prior to each imaging session.

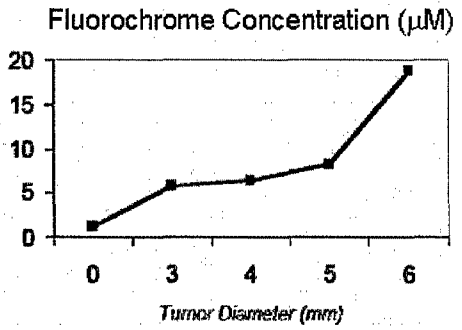

Figure 12: Fluorochrome concentration from the mouse shown in Figure 11 as a function of tumor diameter as measured with calipers.

Using a different probe, consisting of the Her-2 antibody conjugated to Cy5.5, also injected into a transgenic mouse 24-hours prior to imaging, the system was able to resolve a 1 mm tumor (as measured across the diameter of the tumor using calipers; see Figure 13). This finding demonstrates selective probe bio-distribution at early stages of disease progression and represents a significant achievement toward the goal of early detection.

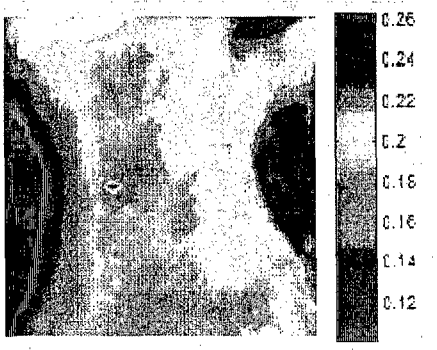

Figure 13: Tomographic slice (z = 1.28 cm) revealing a 1 mm tumor in the right mammary fat pad of mouse.

A2.5: Evaluation of status of achieving year-2 goals

As previously stated we have already made significant progress toward achieving the year 2 goals. We are confident in our optimization of imaging parameters as well as the dose administration of the NIR, cathepsin-activatable probe. What remains ahead for year 2 is completion of the screening study. To continue toward completion of this goal, we will continue to breed mice to achieve the necessary number of subjects. As stated in the grant proposal, we will screen mice as they develop spontaneous tumors of the mammary fat pads. We fully anticipate achieving our target of 40 experimental subjects and 10 controls ahead of schedule.

Additionally, we have already begun correlative work, such as histological examination by hematoxylin and eosin staining, immunohistochemical staining for cathepsins, and Western blotting for cathepsins, to confirm the presence or absence of disease as well as to define the sensitivity thresholds for early detection by FMT and reflectance imaging in-vivo. Therefore, we foresee successful completion of the year-2 goals ahead of schedule, which will enable us to more quickly proceed toward accomplishing the goals for year 3.

Aim 3 (Year 3): To translate animal study findings into clinically-relevant detection schemes.

Consistent with the time plan of the proposal in the second year we will be constructing phantoms that simulate the human breast, both geometrically and in terms of optical properties and we will performing feasibility studies to identify clinical utility.

Key Research Accomplishments

- Implementation of a system that combines 4 modes of illumination/detection namely reflectance, transillumination tomosynthesis and tomography for use in years 2 & 3
- Construction of appropriate phantoms for testing imaging performance.
- Establishment of appropriate animal breast cancer models.
- Establishment of sensitivity limits for the detection of fluorochromes of better than 10nM in 200μL volumes in the center of phantoms with breast optical properties.
- Establishment that tomographic methods are superior to planar imaging methods as a function of depth, optical properties and heterogeneity and is the method of choice for subsequent studies in years 2 & 3. Planar imaging methods will be important for scout studies, where quantification will be necessarily obtained from tomography or tomosynthesis.
- Development of algorithms that are insensitive to background fluorescence and heterogeneity.
- In-vivo imaging of the first animals with spontaneous breast cancer using protease activatable probes to detect cancer

Reportable Outcomes

Journal Publications & Proceedings:

Ntziachristos V, Turner G, Dunham J, Windsor S, Soubret A, Ripoll J Shih HA
"Planar fluorescence imaging using normalized data," *Journal of Bio-optics*, ***in press***, 2005.

Soubret A, Ripoll J, Ntziachristos V, "Accuracy of fluorescence tomography in the presence of heterogeneities: Study of the normalized Born ratio," *IEEE Trans Med Imag*, ***in press***, 2005.

Soubret A, Windsor SD, Turner GM, Ripoll J, Ntziachristos V, "Accuracy of fluorescence tomography in the presence of background fluorescence," *in preparation*, 2005.

Windsor SD, Shih HA, and Ntziachristos, V, "In-vivo fluorescence molecular tomography of mammary adenocarcinomas in transgenic mice bearing an activated c-neu oncogene," *U.S. Army Era of Hope Conference*, Philadelphia, PA, June 2005.

Windsor SD, Shih HA, Weissleder R, Ntziachristos V, "Simultaneous imaging of protease expression and biodistribution in Her-2/neu mice using dual-wavelength fluorescence molecular tomography," *Society of Molecular Imaging Conference*, Cologne, Germany, Sept. 2005.

Presentations:

Windsor SD, "In-vivo fluorescence molecular tomography of mammary adenocarcinomas in transgenic mice bearing an activated c-neu oncogene," U.S. Army Era of Hope Conference, Philadelphia, PA, June 09, 2005.

Conclusions

In this year 1 we achieved all proposed goals and met all milestones. In addition we proceeded in in-vivo studies, originally planned for year 2 with significant success. We were able to identify tumors as early as 2-3mm and we were able to follow their growth as a function of time. In years 2 & 3 we will continue studies towards understanding the targeting ability and early detection based on protease probes and examine the potential for clinical translation.

References

[1] Humphrey LL, Helfand M, Chan BKS, and e. al., "Breast cancer screening: a summary of evidence for the U.S. preventive services task force," *Annals of Internal Medicine*, vol. 137, pp. 347-60, 2002.

[2] Fletcher SW and E. JC., "Clinical practice. Mammographic screening for breast cancer," *N Engl J Med*, vol. 348, pp. 1672-80, 2003.

[3] Arriagada R., Le M. G., Contesso G., Guinebretiere J. M., Rochard F., and S. M., "Predictive factors for local recurrence in 2006 patients with surgically resected small breast cancer," *Ann. Onc.*, vol. 13, pp. 1404 - 1413, 2002.

[4] Arriagada R, Le MG, Rochard F, and C. G., "Conservative treatment versus mastectomy in early breast cancer: patterns of failure with 15 years of follow-up data. Institut Gustave-Roussy Breast Cancer Group," *J Clin Oncol*, vol. 14, pp. 1558-1564, 1996.

[5] Mirza NQ, Vlastos G, Meric F, Buchholz TA, Esnaola N, Singletary SE, Kuerer HM, Newman LA, Ames FC, Ross MI, Feig BW, Pollock RE, McNeese M, Strom E, and H. KK., "Predictors of locoregional recurrence among patients with early-stage breast cancer treated with breast-conserving therapy.," *Ann Surg Oncol.*, vol. 9, pp. 256-65, 2002.

[6] Wallgren A, Bonetti M, Gelber RD, Goldhirsch A, Castiglione-Gertsch M, Holmberg SB, Lindtner J, Thurlimann B, Fey M, Werner ID, Forbes JF, Price K, Coates AS, and C. J, "Risk factors for locoregional recurrence among breast cancer patients: results from International Breast Cancer Study Group Trials I through VII.," *J Clin Oncol.*, vol. 21, pp. 1205-1213, 2003.

[7] Weissleder R and Mahmood U, "Special review: Molecular imaging," *Radiology*, vol. 219, pp. 316-333, 2001.

[8] Weissleder R and Ntziachristos V, "Shedding light onto live molecular targets," *Nat Med*, vol. 9, pp. 123-128, 2003.

[9] Ntziachristos V, Ripoll J, Wang LV, and Weissleder R, "Looking and listening to light: the evolution of whole-body photonic imaging", *Nat Biotech*, vol. 23, pp. 331-320, 2005.

[10] Ntziachristos V, Schellenberger EA, Ripoll J, Yessayan D, Graves E, Bogdanov A, Josephson L, and Weissleder R, "Visualization of antitumor treatment by means of fluorescence molecular tomography with an annexin V-Cy5.5 conjugate," *PNAS*, vol. 101, pp. 12294-12299, 2004.

[11] Ntziachristos V and Chance B, "Probing physiology and molecular function using optical imaging: applications to breast cancer," *Breast Cancer Res*, vol. 3, pp. 41-46, 2001.

[12] Hawrysz DJ and Sevick-Muraca EM, "Developments toward diagnostic breast cancer imaging using near-infrared optical measurements and fluorescent contrast agents," *Neoplasia*, vol. 2, pp. 388-417, 2000.

[13] Colak SB, van der Mark MB, Hooft GW, Hoogenraad JH, van der Linden ES, and Kuijpers FA, "Clinical optical tomography and NIR spectroscopy for breast cancer detection," *IEEE Journal of Selected Topics in Quantum Electronics*, vol. 5, pp. 1143-1158, 1999.

[14] Pogue BW, Poplack SP, McBride TO, Wells WA, Osterman KS, Osterberg UL, and Paulsen KD, "Quantitative Hemoglobin Tomography with Diffuse Near-Infrared Spectroscopy: Pilot Results in the Breast," *Radiology*, vol. 218, pp. 261-266., 2001.

[15] Jakubowski DB, Cerussi AE, Bevilacqua F, Shah N, Hsiang D, Butler J, and Tromberg BJ, "Monitoring neoadjuvant chemotherapy in breast cancer using quantitative diffuse optical spectroscopy: a case study" *J Biomed Opt*, vol. 9, pp. 230-238, 2004.

[16] Weissleder R, "Molecular imaging: exploring the next frontier," *Radiology*, vol. 212, pp. 609-14, 1999.

[17] Ntziachristos V, Yodh AG, Schnall M, and Chance B, "Concurrent MRI and diffuse optical tomography of breast after indocyanine green enhancement," *Proc Nat. Acad Sci U.S.A.*, vol. 97, pp. 2767-72, 2000.

[18] Graves EE, Ripoll J, Weissleder R, Ntziachristos V, "A submillimeter resolution fluorescence molecular imaging system for small animal imaging," *Med Phys*, vol. 30, pp. 901-911, 2003.

[19] Ntziachristos V, Ripoll J, and Weissleder R, "Would near-infrared fluorescence signals propagate through large human organs for clinical studies?," *Optics Letters*, vol. 27, pp. 333-335, 2002.

[20] Weissleder R, Tung CH, Mahmood U, and Bogdanov A, "In vivo imaging of tumors with protease-activated near-infrared fluorescent probes," *Nature Biotech*, vol. 17, pp. 375-8, 1999.

[21] Tung C, Mahmood U, Bredow S, and Weissleder R, "In vivo imaging of proteolytic enzyme activity using a novel molecular reporter," *Cancer Research*, vol. 60, pp. 4953-8, 2000.

[22] Tung C, Bredow S, Mahmood U, and Weissleder R, "Preparation of a cathepsin D sensitive near-infrared fluorescence probe for imaging," *Bioconjug Chem*, vol. 10, pp. 892-6, 1999.

[23] Koblinski JE, Ahram M, and Sloane BF, "Unraveling the role of proteases in cancer," *Clin Chim Acta*, vol. 291, pp. 113-35., 2000.

[24] Yan S, Sameni M, and Sloane BF, "Cathepsin B and human tumor progression," *Biol Chem*, vol. 379, pp. 113-23, 1998.

[25] Sameni M, Elliott E, Ziegler G, and e. al., "Cathepsin B and D are localized at the surface of human breast cancer cells," *Pathol Oncol Res*, vol. 1, pp. 43-53, 1995.

[26] Levicar N, Kos J, Blejec A, and e. al., "Comparison of potential biological markers cathepsin B, cathepsin L, stefin A and stefin B with urokinase and plasminogen activator inhibitor-1 and clinicopathological data of breast carcinoma patients.," *Cancer Detect Prev*, vol. 26, pp. 42-9, 2002.

[27] Ntziachristos V, Weissleder R., "CCD-based scanner for tomography of fluorescent near-infrared probes in turbid media," *Medical Physics*, vol. 29, pp. 803-809, 2002.

Accuracy of Fluorescent Tomography in thePresence of Heterogeneities: Study of theNormalized Born Ratio

Antoine Soubret*, Jorge Ripoll, and Vasilis Ntziachristos

Abstract—**We studied the performance of three-dimensional fluorescence tomography of diffuse media in the presence of heterogeneities. Experimental measurements were acquired using an imaging system consisting of a parallel plate-imaging chamber and a lens coupled charge coupled device camera, which enables conventional planar imaging as well as fluorescence tomography. To simulate increasing levels of background heterogeneity, we employed phantoms made of a fluorescent tube surrounded by several absorbers in different combinations of absorption distribution. We also investigated the effect of low absorbing thin layers (such as membranes). We show that the normalized Born approach accurately retrieves the position and shape of the fluorochrome even at high background heterogeneity. We also demonstrate that the quantification is relatively insensitive to a varying degree of heterogeneity and background optical properties. Findings are further contrasted to images obtained with the standard Born expansion and with a normalized approach that divides the fluorescent field with excitation measurements through a homogeneous medium.**

Index Terms—**Absorption, diffusion theory, fluorescence tomography, molecular imaging.**

I. Introduction

FLUORESCENCE tomography of diffuse media has recently materialized as a quantitative method for imaging novel fluorescent agents with functional or molecular specificity [1]. Tomographic approaches have been developed to overcome significant limitations present in planar optical imaging systems, i.e., systems that front illuminate the animal of interest at an excitation wavelength with a broad photon beam and record fluorescent images of the animals using an appropriate high-pass or bandpass filter. Planar systems yield images that are a superposition of photons emitted from different depths and scattered by the different layers of tissues. In this configuration, depth resolution is not possible and quantification of the fluorescent agent is further complicated by the nonlinear dependence of fluorescence strength on depth and tissue optical properties. Conversely tomography utilizes appropriate photon propagation models that account for nonlinear effects and multiple photon projections and can independently resolve the three-dimensional (3-D) position of fluorochromes and their strength and concentration.

Several groups have offered theoretical and experimental solutions to the tomographic problem [2]–[18]. Inversion is often based on solutions of the diffusion equation obtained either analytically or numerically. Tomographic performance has been evaluated with simulated data [4], [7], [11], [12], and [19]–[23] and with experimental measurements from phantoms [3], [5], [17], [24]. Most algorithmic evaluations, however, have been performed with relatively homogeneous media; typically a small number of fluorochromes is immersed in an otherwise homogeneous fluid with average optical properties similar to those of a target tissue (for example the human breast or a small animal). Therefore, a common criticism of the technique relates to its accuracy and performance in media with high background optical heterogeneity such as tissues.

Developing robust methods that work well at highly heterogeneous diffuse media is important for *in vivo* imaging. We have previously reported on a particular methodology, termed the normalized Born ratio that demonstrated good imaging performance *in vivo*. The corresponding imaging technology, termed fluorescence molecular tomography (FMT) [25], is based on using self calibrated data that divide the fluorescence measurements with corresponding measurements at the excitation wavelength [17]. This normalization scheme can work with analytical or numerical forward solvers and offers significant experimental advantages since it is independent of source strengths, detector gains and coupling efficiency to tissue [17]. Furthermore, it minimizes sensitivity to theoretical errors such as modeling of the boundary conditions or knowledge of the exact tissue optical properties. This normalization scheme was pivotal to the development of the first *in vivo* fluorescence observations of protease up-regulation deep in mouse brains [26] and of tumor treatment in intact animals [27], using appropriate fluorescent probes.

The normalized Born ratio has been shown insensitive to a small number of absorbers in the past [17] using experimental measurements. Furthermore, Roy *et al.* [19] demonstrated that

Manuscript received October 21, 2004; revised July 22, 2005. The work of J. Ripoll was supported in part by the EU Integrated Project Molecular Imaging under Grant LSHG-CT-2003-503259 STREP TRANS-REG and Grant LSHG-CT-2004-502950. This work was supported in part by the U. S. Army Medical Research and Materiel Command under Grant W81XWH-04-01-0239, in part by the National Institute of Health (NIH) under Grant RO1 EB 000750-2, and Grant R33 CA91807, and in part by NASA under Grant BAA-NO1-CO-17-16-32. The Associate Editor responsible for coordinating the review of this paper and recommending its publication was A. Hielscher. *Asterisk indicates corresponding author.*

*A. Soubret is with the Center for Molecular Imaging Research, Massachusetts General Hospital, Harvard Medical School, Charlestown, MA 02129 USA (e-mail: asoubret@hms.harvard.edu).

J. Ripoll is with the Institute of Electronic Structure and Laser, Foundation, for Research and Technology-Hellas, GR 711 10 Heraklion, Greece (e-mail: jripoll@iesl.forth.gr).

V. Ntziachristos is with the Center for Molecular Imaging Research, Massachusetts General Hospital, Harvard Medical School, Charlestown, MA 02129 USA (e-mail: vasilis@helix.mgh.harvard.edu).

Digital Object Identifier 10.1109/TMI.2005.857213

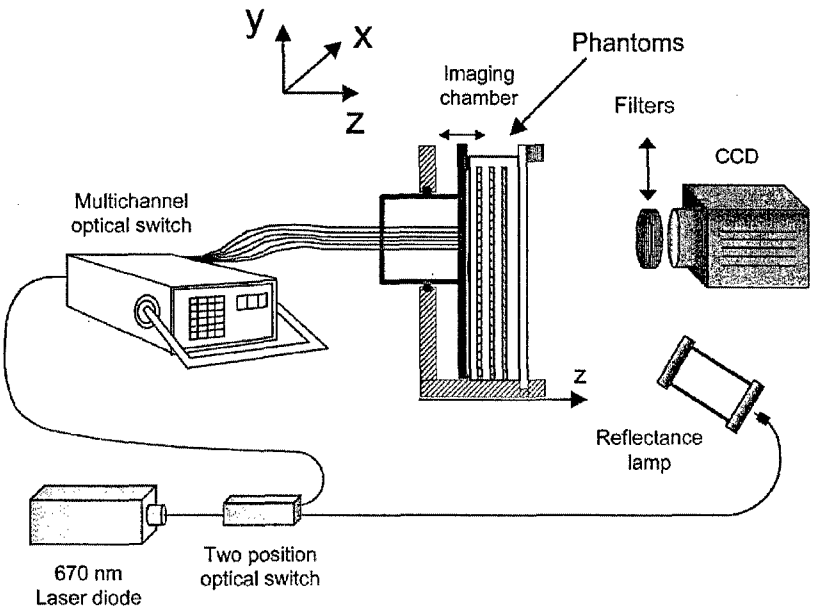

Fig. 1. Experimental setup.

high levels of noise could be added to simulated data without drastically changing the reconstruction performance when using this normalization method. Similarly, Eppstein *et al.* [23] have shown relative insensitivity of fluorescence reconstructions to the spatial variation of optical properties using simulated data.

The work herein focused on experimentally exploring the performance of the normalized Born ratio with increasing background absorption heterogeneity. We employed phantoms containing a varying number of diffuse absorbing tubes with different absorption coefficients surrounding a fluorescent diffuse tube. While it was hypothesized that the normalized Born ratio could perform well at increasing background absorption, our results demonstrated an unexpected robustness even at very high degree of heterogeneity, despite the linear inversion approach used. To contrast these findings, we also examined the performance of 1) the standard Born reconstruction scheme and 2) a normalization scheme that uses calibrated data based on measurements through a homogeneous medium in the absence of the absorbing tubes. Section II, describes the experimental setup and the different heterogeneities considered. Section III presents the forward model and the inversion algorithm employed. Section IV, describes our findings and finally Section V discusses the results and their implications to *in vivo* imaging.

II. Experimental Setup and Phantoms

A. Experimental Setup

A schematic of the FMT acquisition system is shown in Fig. 1 and a detailed description can be found in [16]. A 672 nm wavelength constant wave (CW) laser is routed into a two channel optical switch. This switch allows the system to be used either as a reflectance or tomographic imager. In reflectance mode, the laser beam was expanded with a system of lenses and front-illuminates the object placed in the imaging chamber though a window with anti-reflection coating for the near infrared response. In tomographic mode, a programmable optical switch sequentially directed light in each of the 46 fibers arranged in a space-filling grid pattern used for tomography purposes. The fibers were arranged on a moving plate that can establish a slab-geometry of different thicknesses; here in 1.7 cm. The chamber can be filled with an optical matching fluid with absorbing and scattering properties similar to that of tissues. The light transmitted through the diffuse medium is then recorded with the charge coupled device (CCD) camera at both the excitation and fluorescent wavelength using appropriate filters (for details see [16]).

B. Phantom Geometries

Different configurations of background heterogeneity were constructed by surrounding a single fluorochrome with multiple absorbers of increasing density and absorption. The fluorescent tube was made of a 3-mm-diameter translucent plastic tube containing 1 μM of Cy 5.5 in a solution of 1% intralipid and 50 ppm of India ink. Absorbers were made from the same tube filled with 1% intralipid and different amounts of India ink. All tubes were placed in position using a solid frame that does not interfere with the field of view and immersed in a solution of 1% intralipid and 50 ppm of India ink yielding optical properties $\mu_a^0 = 0.4\ \mathrm{cm}^{-1}$ and $\mu_s' = 8\ \mathrm{cm}^{-1}$ which are characteristic of small animals. Therefore, the fluorescent tube and background medium had the same optical properties.

Three distinct sets of experiments were performed. The first set a) consisted of 12 configurations a1–a12 as shown in Fig. 2. The number of plastic tubes in the chamber is kept constant to eight except for the configuration a12 and the attenuation of the measured signal from one configuration to another is only due to the different concentration of ink in the tubes. The second set of experiments b) consisted of seven configurations and it is similar to the first set of experiments a1–a7 with the exception that tubes with the same optical properties with the background medium are removed from the medium. Therefore, the effect of the plastic tube heterogeneity can be assessed. Those

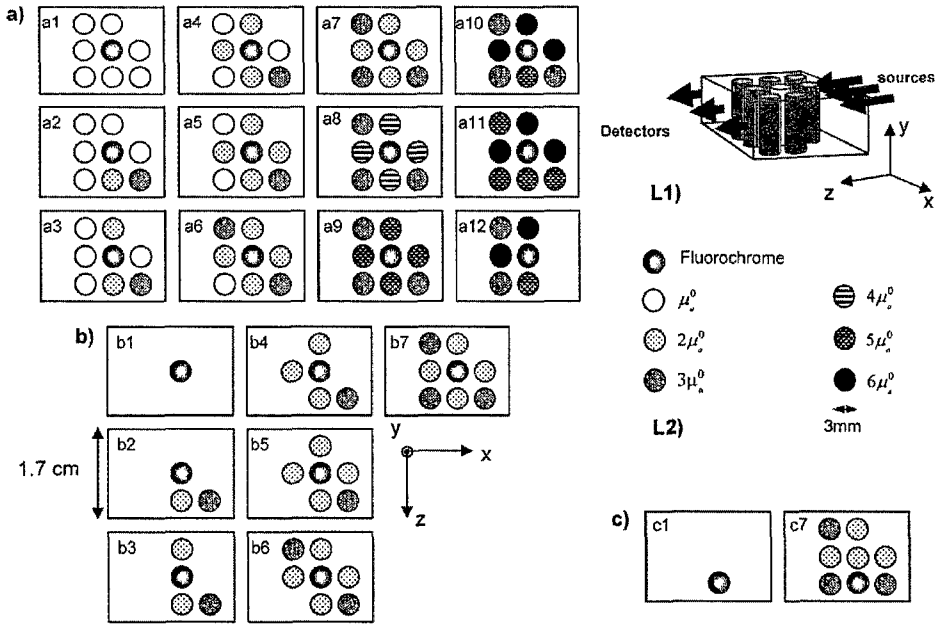

Fig. 2. Horizontal slices (xz plane) of the different phantoms made of a fluorochrome tube surrounded by absorbing tubes. Three sets of experiments a), b), and c) have been used to perform the experiments. The 3-D view of the phantoms a1-a11 and b7 is shown on the view L1). The legend indicating the concentration of ink in the different tubes is depicted on the view L2).

seven configurations are numbered b1–b7 in Fig. 2. The third set of experiments c) imaged a fluorescent tube placed superficially in the diffuse fluid, virtually in contact with the inner side of the imaging window. Two configurations were examined, one for imaging the tube placed in a homogenous background medium and the other with the tube surrounded by seven absorbers. These two configurations are named c1 and c7 in Fig. 2.

Fig. 3 shows an example of the phantoms constructed; in particular it shows reflectance images (photographs) of the phantom set b1 and set b7 of Fig. 2 when there is no background matching fluid (ink-intralipid solution) in the chamber. Photographs at the excitation and the fluorescent channels are shown respectively. As seen, almost no fluorescent signal is detectable in the configuration b7 as compared to the configuration b1 where no absorbers are present. When filling the chamber with the diffuse medium the fluorescent tubes cannot be directly observed with reflectance imaging due to high diffusion and can be revealed only tomographically.

III. Data Normalization and Reconstruction Algorithm

A. Forward Model

The propagation of near-infrared light in tissue is modeled by the diffusion equation which has been shown to work well when sources and detectors are separated by more than a few mean free path lengths [28]. In our experiment, more than 13 mean free path separate the sources and the window imaged by the CCD camera. When the fluorescent tube is inserted in the chamber, the fluorescent field $U_{\text{fluo}}(r_d, r_s)$ detected by the CCD camera at the exit plane is related to the absorption of the fluorochrome $\mu_a^{\text{fluo}}(r_1)$ by (1), shown at the bottom of the page, where $n(r_1) = \eta\,\mu_a^{\text{fluo}}(r_1)$, η the quantum yield of the fluorochrome, r_s, r_d are the location of the source and the detector, $\Theta_{\text{src}}(r_s)$ is the intensity of the source at the fiber exit, Θ_f^{fluo} the attenuation of the fluorescent filter, $\Theta_{\text{det}}(r_d)$ accounts for the detectors gains, $Q_E^{\lambda_{\text{fluo}}}$ is the detector quantum efficiency at the fluorescence wavelength, v is the speed of light in the medium and $D^{\lambda_{\text{fluo}}} = v/3\ \mu_s'$ the diffusion coefficient at the fluorescence wavelength. The Green's function $G_0^{\lambda_{\text{exc}}}(r_1, r_s)$ describes the propagation of the light from the source to the fluorochrome and $G_0^{\lambda_{\text{fluo}}}(r_d, r_1)$ from the fluorochrome to the detector. These functions can be calculated assuming a homogeneous background medium or iteratively using nonlinear inverse algorithms based on finite-differences or finite-element methods [7], [8], [23], [29]. In this paper, we demonstrated imaging performance using a first-order perturbative solution of the diffusion equation assuming a homogeneous background [11]. Boundary conditions were implemented using the extrapolated boundary conditions [30]–[32] and the method of image sources [33] with ten source pairs.

$$U_{\text{fluo}}(r_d, r_s) = Q_E^{\lambda_{\text{fluo}}}\Theta_f^{\text{fluo}} \times \int d^3 r_1 \Theta_{\text{det}}(r_d) G_0^{\lambda_{\text{fluo}}}(r_d, r_1) \frac{v}{D^{\lambda_{\text{fluo}}}} n(r_1) G_0^{\lambda_{\text{exc}}}(r_1, r_s) \Theta_{\text{src}}(r_s) \tag{1}$$

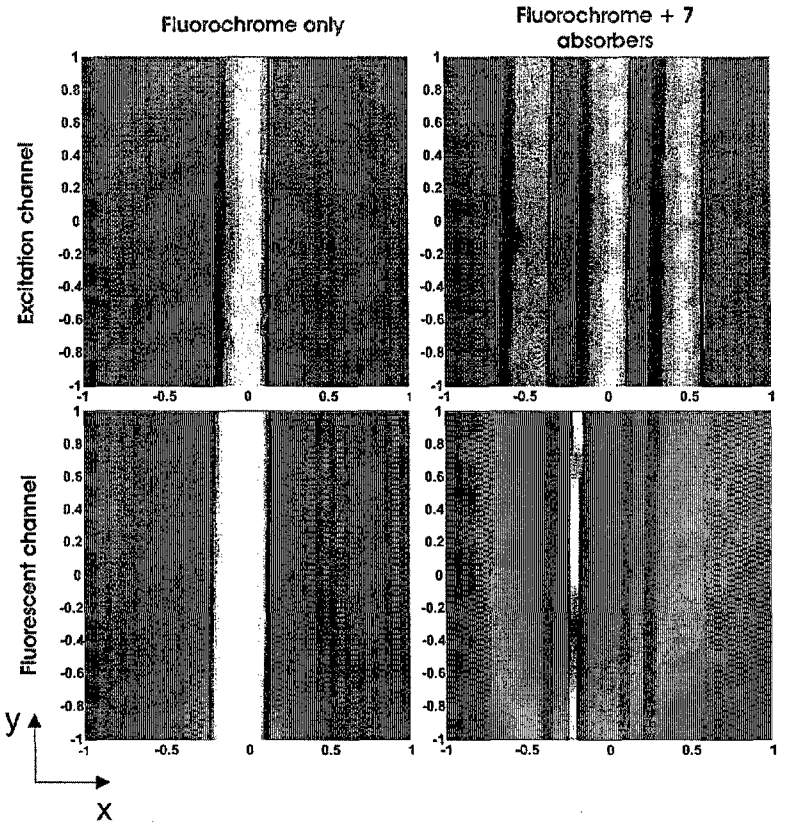

Fig. 3. Reflectance images when only the fluorochrome tube is present in the chamber (configuration b1) and when the fluorochrome tube is surrounded by 7 absorbers tubes(configuration b7). Images are for the excitation channel and the fluorescent channel. The units on the axis x and y are in centimeters.

B. Data Normalization

The use of (1) is experimentally complicated since the parameters $Q_E^{\lambda_{\text{fluo}}}$, $\Theta_{\text{det}}(r_d)$, $\Theta_{\text{src}}(r_s)$ have to be explicitly determined. In addition, the measurements can be complicated by unknown coupling factors of the optical system onto tissue. We have previously suggested the normalized Born ratio, which divides fluorescence measurements with corresponding measurements at the excitation wavelength [17], in order to simplify experimental issues. This is because the normalized Born ratio is effectively independent of the individual gains of source detector pairs and coupling coefficients. Herein, we examine its performance with diffusive media of heterogeneous absorption distribution.

To write the normalized Born ratio, we first decompose the excitation field using Green functions as

$$U_{\text{exc}}(r_d, r_s) = Q_E^{\lambda_{\text{exc}}} \Theta_f^{\text{exc}} \Theta_{\text{det}}(r_d)\, G_0^{\lambda_{\text{exc}}}(r_d, r_s)\, \Theta_{\text{src}}(r_s) \tag{2}$$

where $Q_E^{\lambda_{\text{exc}}}$ is the detector quantum efficiency at the excitation wavelength and Θ_f^{exc} is the attenuation of the filter at the excitation wavelength. Then, the normalized Born ratio $U^{(\text{I})}(r_d, r_s)$ is obtained by dividing (1) by (2), i.e.,

$$\begin{aligned} U^{(\text{I})}(r_d, r_s) &= \frac{U_{\text{fluo}}(r_d, r_s)}{U_{\text{exc}}(r_d, r_s)} \\ &= \alpha_0 \frac{\int d^3 r_1 G_0^{\lambda_{\text{fluo}}}(r_d, r_1) n(r_1) G_0^{\lambda_{\text{exc}}}(r_1, r_s)}{G_0^{\lambda_{\text{exc}}}(r_d, r_s)}. \end{aligned} \tag{3}$$

where

$$\alpha_0 = \frac{Q_E^{\lambda_{\text{fluo}}}}{Q_E^{\lambda_{\text{exc}}}} \frac{\Theta_f^{\text{fluo}}}{\Theta_f^{exc}} \frac{v}{D^{\lambda_{\text{fluo}}}}.$$

The single calibration parameter α_0 depends on generic system characteristics (i.e., filters' and fibers' attenuation, laser power, etc.) and can be simply determined experimentally by measurement of a fluorochrome with known concentration.

In some cases imperfect isolation of the fluorescent filter may result in small remnant signals Θ_{bleed} of the excitation signal propagating in the fluorescent channel. In such occurrence, this "bleed-through" signal is subtracted from the fluorescence field, i.e.,

$$\begin{aligned} \left[U^{(\text{I})}(r_d, r_s)\right]_{\text{measured}} &= \left[\frac{U_{\text{fluo}}(r_d, r_s) - \Theta_{\text{bleed}} U_{\text{exc}}(r_d, r_s)}{U_{\text{exc}}(r_d, r_s)}\right]_{\text{measured}}. \end{aligned} \tag{4}$$

The coefficient Θ_{bleed} can be experimentally determined by illuminating the chamber filled with any nonfluorescent diffusing medium and calculating the ratio of counts measured at the fluorescent channel over the counts measured at the intrinsic channel [16].

As it will appear in the following, this Born ratio does not only offer convenient calibration but also significantly minimizes the sensitivity to the presence of background optical heterogeneities. The following three different data schemes were

examined here in relation to their performance with increased background heterogeneity.

- Normalization I, which employed the normalized Born ratio as shown in (4). The excitation light field used was obtained from the heterogeneous medium containing the fluorochrome and the different combinations of absorbers.
- Normalization II, which employed a normalized Born field $U^{(\mathrm{II})}(r_d, r_s)$, whereas the excitation light field $U_{\mathrm{exc}}^{(\mathrm{homog})}(r_d, r_s)$ is measured from a homogeneous background medium, i.e., from the chamber filled only with a homogeneous solution of intralipid and ink in the absence of absorbers or fluorochromes. This fluid was identical to the fluid used as a background medium in the heterogeneous case. The field employed in this normalization can be written similarly to (4) as

$$\left[U^{(\mathrm{II})}(r_d, r_s)\right]_{\mathrm{measured}} = \left[\frac{U_{\mathrm{fluo}}(r_d, r_s) - \Theta_{\mathrm{bleed}} U_{\mathrm{exc}}^{(\mathrm{homog})}(r_d, r_s)}{U_{\mathrm{exc}}^{(\mathrm{homog})}(r_d, r_s)}\right]_{\mathrm{measured}}. \quad (5)$$

- Normalization III, which employed a standard Born field $U^{(\mathrm{III})}(r_d, r_s)$ (see [11]). This field is normalized only with source strength $g_0(r_s)$ at each position r_s since the use of individual fibers in the system described above often leads to variability in optical transmittance from fiber to fiber due to differences in coupling losses in the optical switch and elsewhere. The field employed in this normalization can be written as

$$\left[U^{(\mathrm{III})}(r_d, r_s)\right]_{\mathrm{measured}} = \left[\frac{U_{\mathrm{fluo}}(r_d, r_s) - \Theta_{\mathrm{bleed}} U_{\mathrm{exc}}^{(\mathrm{homog})}(r_d, r_s)}{g_0(r_s)}\right]_{\mathrm{measured}}. \quad (6)$$

The factor $g_0(r_s)$ is calculated as the maximum average intensity of photon fields propagating though the homogeneous medium for the different sources employed so that $g_0(r_s) = \max_{r_d}(U_{\mathrm{exc}}^{(\mathrm{homog})}(r_d, r_s))$. This normalization works on the basis that $g_0(r_s)$ is proportional to the intensity of the source $\Theta_{\mathrm{src}}(r_s)$ located at r_s. This method normalizes, therefore, the measurements to the source strength but it does not take into account the spatial dependence of the measured excitation field since $g_0(r_s)$ only depends on the source position r_s and not on the location r_d of the detector.

C. Reconstruction

To solve the inverse problem, we discretized the integral equation (3) and evaluated the fluorescent term $n(r_1)$ on a 3-D grid of size N_x, N_y, N_z. For each source-detector pair (r_d^i, r_s^i) and each point $(r^j)_{j=1\ldots N_x N y N_z}$ on the grid, the weight function W_{ij}^{nB} connecting the measurement $U_i^{nB} = U^{nB}(r_d^i, r_s^i)$ to the unknowns $n_j = n(r^j)$ is

$$W_{ij}^{nB} = \delta V \frac{G_0^{\lambda_{\mathrm{fluo}}}(r_{d,}^i r^j) G_0^{\lambda_{\mathrm{exc}}}(r^j, r_s^i)}{G_0^{\lambda_{\mathrm{exc}}}(r_d^i, r_s^i)} \quad (7)$$

where δV is the volume of each voxel of the grid.

Then the discretized linear forward problem can be written as

$$[U_i^{(\mathrm{I})}]_{\mathrm{measured}} = \alpha_0 \sum_j W_{ij}^{nB} n_j. \quad (8)$$

As we do not take into account the heterogeneities in the evaluation of the Green functions the same weight matrix is used when the Normalization II is considered

$$[U_i^{(\mathrm{II})}]_{\mathrm{measured}} = \alpha_0 \sum_j W_{ij}^{nB} n_j. \quad (9)$$

For implementing the normalization III, fluorescent data are normalized only with the corresponding source strengths. Consequently the weight function is not normalized in this case by the source-detector Greens function and the forward problem is written as

$$W_{ij}^{B} = \delta V G_0^{\lambda_{\mathrm{fluo}}}(r_{d,}^i r^j) G_0^{\lambda_{\mathrm{exc}}}(r^j, r_s^i)$$

and the corresponding forward problem is written as

$$[U_i^{(\mathrm{III})}]_{\mathrm{measured}} = \tilde{\alpha}_0 \sum_j W_{ij}^{B} n_j$$

where $\tilde{\alpha}_0$ is the corresponding normalization factor for the Born normalization

$$\tilde{\alpha}_0 = Q_E^{\lambda_{\mathrm{fluo}}} \Theta_f^{\mathrm{fluo}} \frac{v}{D^{\lambda_{\mathrm{fluo}}}}.$$

The 3-D mesh used for the reconstructions was $N_x = 29$, $N_y = 27$, $N_z = 18$ for a field of view of 2.8 cm × 2.6 cm with a depth equal to the thickness of the slab (i.e., 1.7 cm). The voxel size was 0.1 cm × 0.1 cm × 0.1 cm. A subsampled set of measurements was extracted from the 512 × 512 pixels image acquired by the CCD camera by averaging square regions. This process results in a total of 30 × 30 detectors available for each measurement. For each source detector pair (which consists of 30 × 30 × 46 = 41 400 values), a threshold was applied to select only the measurements with a high signal to noise ratio (i.e., around 10 000–15 000 values are effectively used). The fluorescence n_j is obtained in calculating the Moore-Penrose pseudoinverse with an algebraic reconstruction technique (ART) with a random projection access order [34]. The number of ART iterations was fixed to 20. Several relaxation parameters have been tested, and as noticed by Herman [35] a strong under-relaxation scheme gives the best result in terms of solution stability. In the following reconstructions, we have used the value 0.03 for the relaxation parameter.

D. Image Analysis

For quantification purposes the reconstructed values reported for the fluorescent tube were calculated as a summation of the fluorescence intensities reconstructed, above a threshold, for all voxels contained within a selected volume of interest (VOI). The threshold was empirically set to 5% of the maximum value reconstructed for the configuration a1, for each of the three normalizations, and was kept constant for subsequent reconstructions. The VOI selected contained all voxels reconstructed, expect for the ones belonging to the first two and the last two vertical (coronal) slices, i.e the slices that are parallel to the x–y plane and are respectively close to the source plane and the

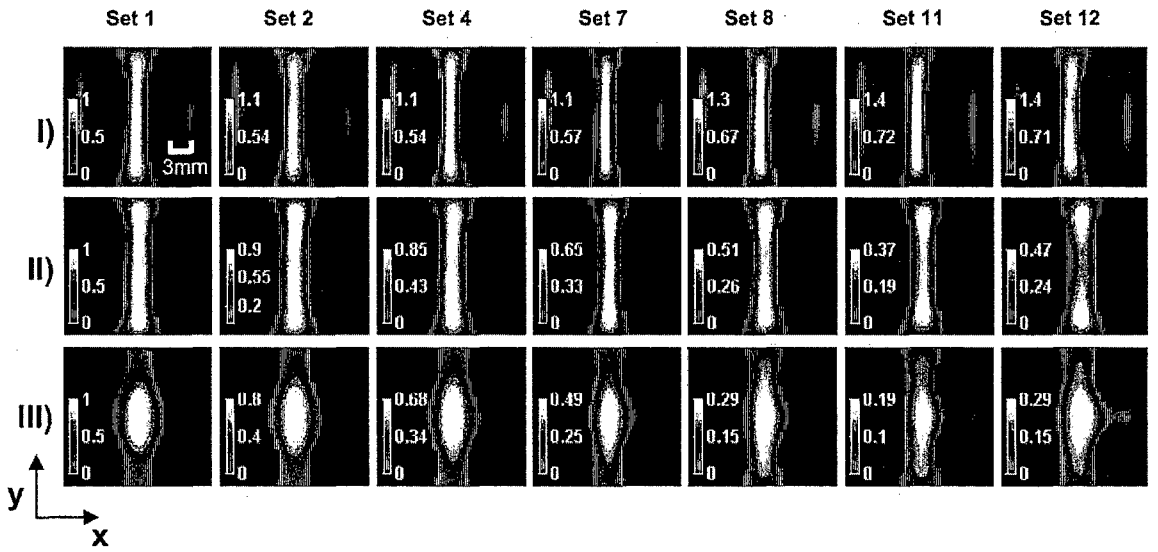

Fig. 4. Vertical (coronal) slices along the x-y plane at the depth z = 0.65 cm showing the reconstructed fluorochrome tube for the configurations set a1, a2, a4, a7, a8, a11, a12. The first row I) has been obtained with the Normalization I, the second row II) with the Normalization II and the third row III) with the Normalization III as described in Section III–A. For each row, the fluorescence reconstructed values for the configuration a1-a12 have been divided by the maximum value for the configuration a1.

imaging window. This is because some artifacts tend to appear close to the sources and detectors. These artifacts were thus excluded from the quantification calculations.

To evaluate quantification errors as a function of normalization method and configuration, one of the configurations examined was selected as a reference and the corresponding summed fluorescence intensity reconstructed was fixed to 1 (in arbitrary units). All other reconstructed summed intensities were divided with this reference value, to record the relative change in quantification, as result of the normalization method selected and the absorber configuration examined. Results are plotted by selecting two different configurations as references, i.e., the configuration a1, a6 for the set of experiment a) and b1, b4 for the set b).

To assess overall image quality, each reconstructed image was attributed with a score (from 1 to 10) based on localization and shape accuracy. These parameters were visually evaluated from two imaging scientists at the post-graduate level trained for more than five years to assess imaging quality of diffusive images by superimposing reconstructed images on the tube photographs obtained under identical positional parameters and with the same optical system (prior to adding surrounding absorbers and the diffuse fluid). This scoring method was used for evaluating the relative qualitative imaging performance of the different normalization methods employed.

IV. Experimental Results and Reconstruction

A. Imaging at the Presence of Absorbing Heterogeneity

Fig. 4 shows vertical reconstructed slices (coronal slices) at the depth z = 0.65 cm of the 3-D reconstructed tube for the configurations a1, a2, a4, a7, a8, a11, and a12. Each row in the image corresponds to reconstructed data obtained with the Normalizations I, II, and III, respectively. The results shown for different configurations are scaled using the configuration a1 as reference for each normalization scheme I, II, and III. Calibration of the constants α_0 and $\tilde{\alpha}_0$ can be used to convert the data to concentration units; however, this was not practiced herein since it does not bear relevance to the particular goals of the study.

Evident on the images is that the fluorescent tube is well reconstructed at all levels of absorption variation attempted when employing the normalization I. The tube position and size are well reconstructed as background absorption heterogeneity is increased. The reconstructions produced using the normalization II are also fairly accurate but the shape of the tube is distorted and right shifted for high absorption as clearly visible on the set a12. Finally, imaging with the normalization III attains the largest distortion since the reconstructed images are strongly affected in shape, quantification and position. In particular, the fluorescence intensity reconstructed is stronger at the center of the reconstructed field. Furthermore, the asymmetry of the configuration a12, where the absorbers are located only on one side of the fluorochrome, is evident on the corresponding reconstruction.

All schemes examined yielded variation on the fluorescence intensity reconstructed. Fig. 5 summarizes the quantification variation for the different configurations examined and the data normalization employed. When configuration a1 was used as reference, the subsequent reconstructed data demonstrated a gradual overestimation of the fluorescence intensity reconstructed for normalization I. This overestimation is of the order of 10% for the first seven cases (set a1 to a7). As the absorption further increases, the reconstructed value is overestimated by up to 15%. In contrast, an underestimation is observed for normalizations II and III. Here, the underestimation exceeds 60% for the most absorbing cases.

Fig. 5(b) re-plots this data, assuming configuration a6 as a reference. This plot represents better the *in vivo* situation where some degree of heterogeneity is always present. Based on these plots it is noted that Normalization I generally leads

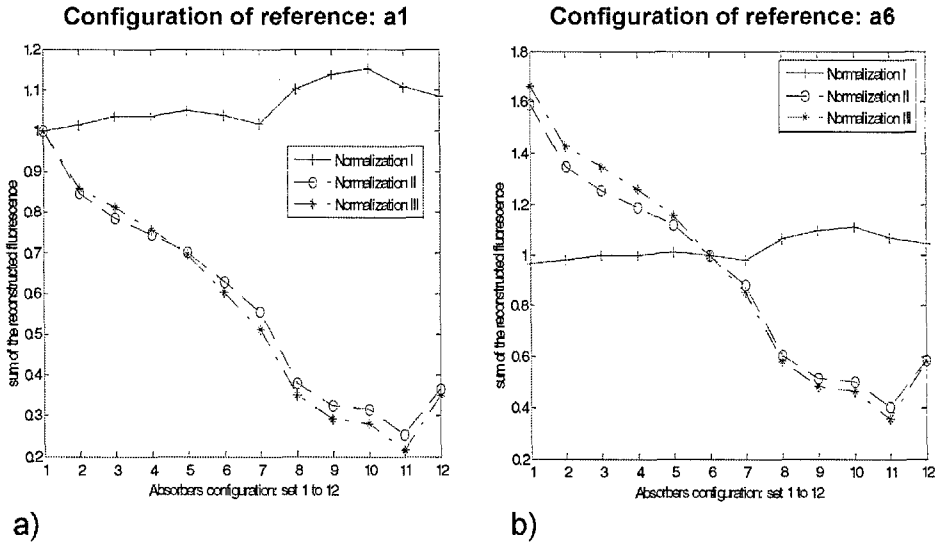

Fig. 5. Relative change in fluorescence strength reconstructed for the different data normalizations as a function of configurations a1–a12. (a) Relative quantification change as a function of background heterogeneity assuming configuration a1 as reference. (b) Re-plot of the data in (a) assuming the configuration a6 as reference.

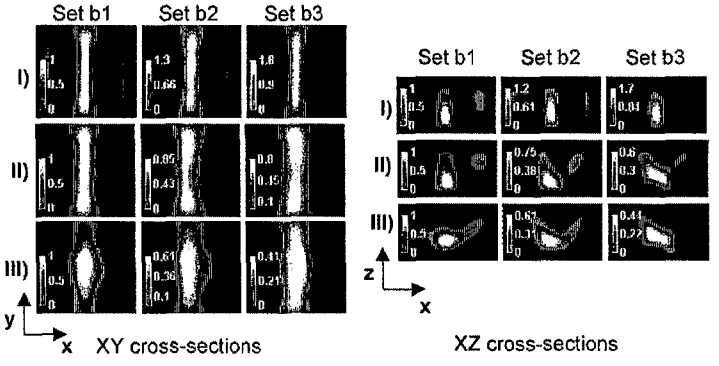

Fig. 6. Vertical (coronal) slices along the x-y plane at the depth z = 0.65 cm and horizontal (axial) slices along the x-z at the position y = 0 cm showing the reconstructed fluorescent tube for the configurations b1–b3. The first row I) has been obtained with the normalization I, the second row II) with the normalization II and the row III) with the normalization III. For each row, the images have been divided by the maximum value for the configuration b1.

to a fluorochrome strength over-estimation for increasing background absorption heterogeneity and to an underestimation for decreasing background heterogeneity. Correspondingly, Normalizations II and III result in overestimation for decreasing background absorption heterogeneity and to an underestimation for increasing background heterogeneity. This result points to the practical and intuitive conclusion that algorithm calibrations should be performed in heterogeneous media to reduce quantification errors for background absorption variations. We have also performed reconstructions using a forward model that assumed different absorption coefficients that match the average optical properties for each configuration examined. This yielded similar observations, especially for the normalization methods I and II due to the relative insensitivity of the ratio methods to the exact knowledge of the optical properties.

B. *Effect of Semi-Translucent Interfaces*

Fig. 6 shows the vertical reconstructed slices (coronal slices) at the depth z = 0.65 cm and horizontal slices (axial slices) at the position y = 0 cm for sets b1 – b3. Similar imaging performance was obtained for the other configurations as well. All images are referenced to the configuration b1, i.e., each of the image shown was divided by the maximum value obtained for the configuration b1. Similarly to Fig. 4, the results depict that the Normalization I reconstruction accurately reconstructs the location and shape of the tube on the coronal views. Normalization II and III are more sensitive to the background optical variation since the yield less accurate shape reconstructions compared to the ones obtained with Normalization I. The effects of the background heterogeneity seen herein are more significant than the ones seen in Fig. 4 since measurements are affected by both absorption and refraction index changes from one configuration to another due to the introduction of the semi-translucent plastic tubes. Interestingly, the reconstruction shows less distortion for higher degree of heterogeneity for all normalization schemes (results not shown) possibly because of the relative symmetry that is restored in the medium when more absorbing tubes are added.

These effects are also evident on the corresponding axial images (XZ cross-sections) shown in Fig. 6. Since the scanner operates on a slab geometry, the resolution along z is compromised in relation to the resolution achieved in the x–y plane. There-

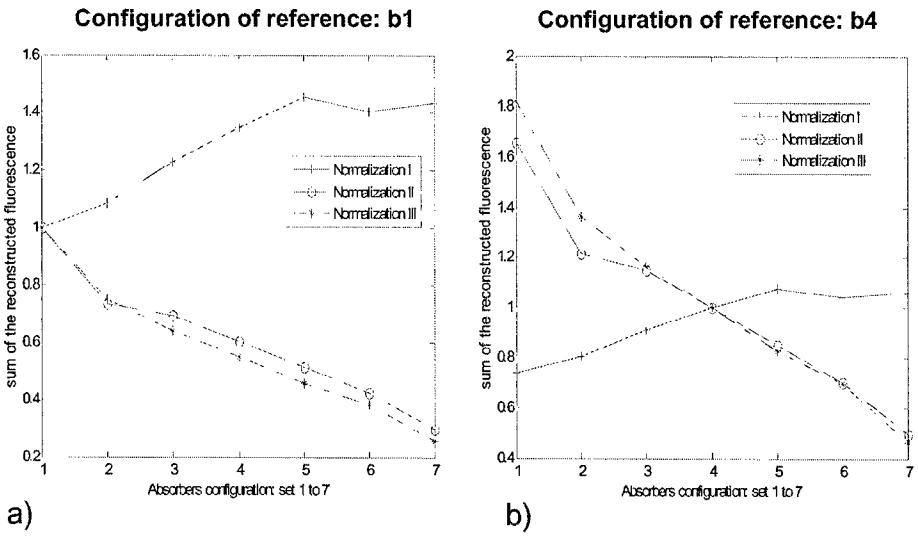

Fig. 7. Relative change in fluorescence strength reconstructed for the three normalization schemes studied as a function of configurations b1–b7. (a) Results plotted using the configuration b1 as reference. (b) Results plotted using configuration b4 as the reference.

fore, the tube is reconstructed elongated using Normalization I but its x–y location is well resolved. However, Normalization II and III give notable distortion in the tube reconstructed.

Fig. 7 depicts the quantification trends observed for the different heterogeneity configurations examined. Two configurations (b1 and b4) were used as reference, i.e., the fluorescence strength calculated for b1 or b4 was used to divide all other quantification calculation obtained. Findings indicate a similar performance as the one seen in Fig. 5. The normalization I over-estimates the fluorescence strength for increasing background heterogeneity and underestimates it for decreasing heterogeneity. The opposite is observed for Normalizations II and III. However, the errors in quantification are stronger than in the cases examined in Fig. 5 due to the added effect of the semi-translucent interfaces. In particular when the reference configuration b1 is used, we observe that the normalization I yielded overestimation by more than 35% when more than four absorbers were present. Correspondingly, we observed an underestimation of up to 65% compared to the reference reconstruction when using normalization II and III.

C. Effect of Depth

To examine the dependence of the methods to depth, we placed the tube adjacent to the front imaging window and examined the reconstruction performance assuming a homogeneous background and a highly heterogeneous background employing seven objects as shown in Fig. 2(c). The reconstructions using the normalization I are shown in Fig. 8. In this case, the background heterogeneity bears insignificant effects on the image quality both in terms of shape and quantification.

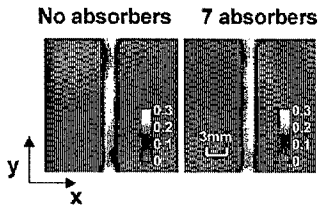

Fig. 8. Fluorescence reconstruction using the normalization I when the fluorochrome is placed superficially, i.e., close to the detector plane (see Fig. 2). The first column is the reconstruction for the configuration c1 without any absorbers and the second column for the configuration c7 when 7 absorbers are present. The vertical (coronal) slice along the x–y plane is at depth z = 1.6 cm. The reconstructed values are in arbitrary units.

V. Discussion and Conclusion

In this paper, we examined the effect of background optical heterogeneity on fluorescence tomography performance. This work is strongly linked to imaging of fluorochromes in tissues and comes to address concerns associated with the *in vivo* performance of fluorescence tomography, in particular when using linear solutions derived on the assumption of photon propagation in homogenous diffuse media.

The results demonstrate robust performance even at high background optical variations, especially when employing the Normalization I. This robustness was demonstrated using absorbing variations over a wide variety of optical properties and spatial distributions. Good imaging performance was also demonstrated for the case where the effect of semi-translucent plastic tubes was progressively introduced in the measurements. The normalization II demonstrated good imaging quality only when the background absorption was varied, but it was more sensitive to the changes introduced by the translucent tubes compared to the performance of normalization I. Generally, these normalized methods are quite insensitive to the background optical properties used in the reconstructions. It is, however, possible that these results could be further improved by adapting the optical properties used in the reconstruction to the exact "average" optical properties of the tissue measured. In addition, the results obtained using the normalization II could be improved if a separate matching fluid was employed, with the average optical properties of each of the different configurations examined. However, this practice would be tedious to

implement in *in vivo* measurements. Finally, the normalization III gave overall the worse imaging performance in terms of localization, shape accuracy, and reconstruction owing to the spatial variation of the background optical properties and other experimental and theoretical uncertainties.

Our observations are based on CW measurements due to their relevance to a scanner developed for small animal FMT imaging [16]. Absorption heterogeneities cannot be distinguished with high contrast from scattering heterogeneities [36], [37] when using CW measurements purely; therefore, the study of absorption heterogeneities in this paper should map the effects of contrast from attenuation in general. For this reason instead of repeating measurements with scattering diffuse inhomogeneities we opted to examine the effects of the virtually semi-diffusive plastic surfaces composing the tubes employed in the study. This heterogeneity can be seen as simulating different tissue membranes, layers of adipose tissue or even fluid layers as common in brain measurements due to the cerebrospinal fluid [38], [39] although the relative geometry of these semi-diffusive surfaces will also influence the result. It was experimentally observed that the effects of the tubes yielded significant changes in the reconstructed data, and these effects were more evident in the reconstructions using the normalization II and III. However, it is expected that most *in vivo* measurements do not have such high density of semi-diffusive regions, especially in comparison to the highly heterogeneous configurations (b5–b7) examined herein

The normalization I demonstrated better quantification accuracy than the other two methods although the overall quantification error depended on the heterogeneous arrangement and optical property combination of heterogeneity and background calibration medium (for normalization II). Furthermore, it was observed that superficially seated objects are reconstructed with superior accuracy than deep-seated objects. Therefore, the observations in Figs. 4–7 correspond to a worse case scenario. This is intuitively correct since the intrinsic field measurement maps almost identically the excitation field for the surface fluorochromes and, therefore, the effects of background heterogeneity cancel out when using normalization I. In addition, the insensitivity of the normalization I and II to unknown experimental and modeling inconsistencies, such as the unknown gains and attenuations of the system and inaccuracies of the diffusion approximation is a significant advantage of normalization methods leading to reduced experimental complexity and better imaging performance. The normalization III does not attain this advantage and, therefore, reconstructions become sensitive to system calibration and accuracy of the theoretical model used. In our case this method resulted in compromised image quality even when imaging the fluorochrome tube alone. It is possible that these distorted reconstructions are due to inaccurate modeling of the source distribution which is assumed herein isotropic, an assumption that is not entirely consistent with the exact photon propagation of the incident beam in the first few millimeters of propagation. Since the normalization I and II are both independent of the source term they are not sensitive to such theory-experiment mismatch.

Finally, while the current study examined the effects of optical property variation, it is expected that inhomogeneous fluorescence distribution will further add to the complexity of the problem and such investigations are currently considered.

In conclusion, we have found that inversion models based on perturbation solutions of the diffusion approximation can yield robust imaging performance even at increased background optical heterogeneity when appropriate data normalization is considered. Such methods offer superior imaging performance in *in vivo* application compared to nonnormalized methods when using linear inversion schemes. This study demonstrated that the use of the normalization I (normalized Born ratio) approach can yield quantification accuracy of the order of $\pm 10\%$ as a function of background optical property heterogeneity, especially when calibrations are obtained in heterogeneous media. While the experiments performed were modeled after the dimensions, optical properties and spatially varying heterogeneity seen in small animal optical imaging, the normalization methods investigated in this work could be potentially beneficial for clinical imaging as well, for example breast optical tomography.

ACKNOWLEDGMENT

The authors would like to thank Dr. G. Turner, Dr. G. Zacharakis, D. Yessayan, and A. Issa-Samarou for helpful discussions and assistance with experiments.

REFERENCES

[1] V. Ntziachristos, J. Ripoll, L. H. V. Wang, and R. Weissleder, "Looking and listening to light: The evolution of whole-body photonic imaging," *Nat. Biotechnol.*, vol. 23, pp. 313–320, 2005.

[2] B. B. Das, F. Liu, and R. R. Alfano, "Time-resolved fluorescence and photon migration studies in biomedical and model random media," *Rep. Prog. Phys.*, vol. 60, pp. 227–292, 1997.

[3] J. H. Chang, H. L. Graber, and R. L. Barbour, "Imaging of fluorescence in highly scattering media," *IEEE Trans. Biomed. Eng.*, vol. 44, no. 9, pp. 810–822, Sep. 1997.

[4] M. J. Eppstein, D. J. Hawrysz, A. Godavarty, and E. M. Sevick-Muraca, "Three-dimensional, Bayesian image reconstruction from sparse and noisy data sets: Near-infrared fluorescence tomography," *Proc. Nat. Acad. Sci.*, vol. 99, pp. 9619–9624, 2002.

[5] A. Godavarty, M. J. Eppstein, C. Y. Zhang, S. Theru, A. B. Thompson, M. Gurfinkel, and E. M. Sevick-Muraca, "Fluorescence-enhanced optical imaging in large tissue volumes using a gain-modulated ICCD camera," *Phys. Med. Biol.*, vol. 48, pp. 1701–1720, 2003.

[6] H. B. Jiang, "Frequency-domain fluorescent diffusion tomography: A finite-element-based algorithm and simulations," *Appl. Optics*, vol. 37, pp. 5337–5343, 1998.

[7] A. D. Klose and A. H. Hielscher, "Fluorescence tomography with simulated data based on the equation of radiative transfer," *Opt. Lett.*, vol. 28, pp. 1019–1021, 2003.

[8] J. Lee and E. M. Sevick-Muraca, "Three-dimensional fluorescence enhanced optical tomography using referenced frequency-domain photon migration measurements at emission and excitation wavelengths," *J. Opt. Soc. Am. A*, vol. 19, pp. 759–771, 2002.

[9] V. V. Lyubimov, "Principles of fluorescence laser tomography of strongly scattering media," *Opt. Spectrosc+.*, vol. 88, pp. 282–285, 2000.

[10] A. B. Milstein, S. Oh, K. J. Webb, C. A. Bouman, Q. Zhang, D. A. Boas, and R. P. Millane, "Fluorescence optical diffusion tomography," *Appl. Optics*, vol. 42, pp. 3081–3094, 2003.

[11] M. A. Oleary, D. A. Boas, X. D. Li, B. Chance, and A. G. Yodh, "Fluorescence lifetime imaging in turbid media," *Opt. Lett.*, vol. 21, pp. 158–160, 1996.

[12] R. Roy and E. M. Sevick-Muraca, "Three-dimensional unconstrained and constrained image-reconstruction techniques applied to fluorescence, frequency-domain photon migration," *Appl. Optics*, vol. 40, pp. 2206–2215, 2001.

[13] E. M. Sevick-Muraca, J. S. Reynolds, T. L. Troy, G. Lopez, and D. Y. Paithankar. "Fluorescence lifetime spectroscopic imaging with measurements of photon migration," in *Advances in Optical Biopsy and Optical Mammography*. New York: New York Academy Sciences, 1998, vol. 838, Annals of the New York Academy of Sciences, pp. 46–57.

[14] E. M. Sevick-Muraca, J. P. Houston, and M. Gurfinkel, "Fluorescence-enhanced, near infrared diagnostic imaging with contrast agents," *Curr. Opin. Chem. Biol.*, vol. 6, pp. 642–650, 2002.

[15] J. Wu, Y. Wang, L. Perelman, I. Itzkan, R. R. Dasari, and M. S. Feld, "Time-resolved multichannel imaging of fluorescent objects embedded in turbid media," *Opt. Lett.*, vol. 20, pp. 489–491, 1995.

[16] E. E. Graves, J. Ripoll, R. Weissleder, and V. Ntziachristos, "A submillimeter resolution fluorescence molecular imaging system for small animal imaging," *Med. Phys.*, vol. 30, pp. 901–911, 2003.

[17] V. Ntziachristos and R. Weissleder, "Experimental three-dimensional fluorescence reconstruction of diffuse media by use of a normalized Born approximation," *Opt. Lett.*, vol. 26, pp. 893–895, 2001.

[18] V. Ntziachristos, C. Bremer, and R. Weissleder, "Fluorescence imaging with near-infrared light: New technological advances that enable *in vivo* molecular imaging," *Eur. Radiol.*, vol. 13, pp. 195–208, 2003.

[19] R. Roy, A. Godavarty, and E. M. Sevick-Muraca, "Fluorescence-enhanced optical tomography using referenced measurements of heterogeneous media," *IEEE Trans. Med. Imag.*, vol. 22, no. 7, pp. 824–836, Jul. 2003.

[20] M. J. Eppstein, F. Fedele, J. Laible, C. Zhang, A. Godavarty, and E. M. Sevick-Muraca, "A comparison of exact and approximate adjoint sensitivities in fluorescence tomography," *IEEE Trans. Med. Imag.*, vol. 22, no. 10, pp. 1215–1223, Oct. 2003.

[21] R. Roy and E. M. Sevick-Muraca, "Truncated Newton's optimization scheme for absorption and fluorescence optical tomography: Part II reconstruction from synthetic measurements," *Opt. Express*, vol. 4, pp. 372–382, 1999.

[22] D. J. Hawrysz, M. J. Eppstein, J. W. Lee, and E. M. Sevick-Muraca, "Error consideration in contrast-enhanced three-dimensional optical tomography," *Opt. Lett.*, vol. 26, pp. 704–706, 2001.

[23] M. J. Eppstein, D. E. Dougherty, D. J. Hawrysz, and E. M. Sevick-Muraca, "Three-dimensional Bayesian optical image reconstruction with domain decomposition," *IEEE Trans. Med. Imag.*, vol. 20, no. 3, pp. 147–163, Mar. 2001.

[24] E. Shives, Y. Xu, and H. B. Jiang, "Fluorescence lifetime tomography of turbid media based on an oxygen-sensitive dye," *Optics Express*, vol. 10, pp. 1557–1562, 2002.

[25] V. Ntziachristos, A. G. Yodh, M. Schnall, and B. Chance, "Concurrent MRI and diffuse optical tomography of breast after indocyanine green enhancement," *Proc. Nat. Acad. Sci.*, vol. 97, pp. 2767–2772, 2000.

[26] V. Ntziachristos, C. Tung, C. Bremer, and R. Weissleder, "Fluorescence-mediated tomography resolves protease activity *in vivo*," *Nat. Med.*, vol. 8, pp. 757–760, 2002.

[27] V. Ntziachristos, E. A. Schellenberger, J. Ripoll, D. Yessayan, E. Graves, A. Bogdanov, L. Josephson, and R. Weissleder, "Visualization of antitumor treatment by means of fluorescence molecular tomography with an annexin V-Cy5.5 conjugate," *Proc. Nat. Acad. Sci.*, vol. 101, pp. 12 294–12 299, 2004.

[28] A. Kienle and M. S. Patterson, "Improved solutions of the steady-state and the time-resolved diffusion equations for reflectance from a semi-infinite turbid medium," *J. Opt. Soc. Am. A*, vol. 14, pp. 246–254, 1997.

[29] M. J. Eppstein, D. E. Dougherty, T. L. Troy, and E. M. Sevick-Muraca, "Biomedical optical tomography using dynamic parameterization and Bayesian conditioning on photon migration measurements," *Appl. Optics*, vol. 38, pp. 2138–2150, 1999.

[30] R. Aronson, "Boundary-conditions for diffusion of light," *J. Opt. Soc. Am. A*, vol. 12, pp. 2532–2539, 1995.

[31] G. W. Faris, "Diffusion equation boundary conditions for the interface between turbid media: A comment," *J. Opt. Soc. Am. A*, vol. 19, pp. 519–520, 2002.

[32] R. C. Haskell, L. O. Svaasand, T. T. Tsay, T. C. Feng, and M. S. McAdams, "Boundary-conditions for the diffusion equation in radiative-transfer," *J. Opt. Soc. Am. A*, vol. 11, pp. 2727–2741, 1994.

[33] M. S. Patterson, B. Chance, and B. C. Wilson, "Time resolved reflectance and transmittance for the noninvasive measurement of tissue optical-properties," *Appl. Optics*, vol. 28, pp. 2331–2336, 1989.

[34] X. Intes, V. Ntziachristos, J. P. Culver, A. Yodh, and B. Chance, "Projection access order in algebraic reconstruction technique for diffuse optical tomography," *Phys. Med. Biol.*, vol. 47, pp. N1–N10, 2002.

[35] G. T. Herman, "Algebraic reconstruction techniques in medical imaging," in *Medical Imaging Systems Techniques and Applications, Gordon and Breach International Series in Engineering, Technology, and Applied Science*, C. T. Leondes, Ed. Amsterdam, The Netherlands: Gordon and Breach Science Publishers, 1997, pp. 1–42.

[36] H. B. Jiang, K. D. Paulsen, and U. L. Osterberg, "Optical image reconstruction using DC data: Simulations and experiments," *Phys. Med. Biol.*, vol. 41, pp. 1483–1498, 1996.

[37] H. B. Jiang, K. D. Paulsen, U. L. Osterberg, and M. S. Patterson, "Improved continuous light diffusion imaging in single- and multi-target tissue-like phantoms," *Phys. Med. Biol.*, vol. 43, pp. 675–693, 1998.

[38] H. Dehghani, D. T. Delpy, and S. R. Arridge, "Photon migration in non-scattering tissue and the effects on image reconstruction," *Phys. Med. Biol.*, vol. 44, pp. 2897–2906, 1999.

[39] A. H. Hielscher, A. Y. Bluestone, G. S. Abdoulaev, A. D. Klose, J. Lasker, M. Stewart, U. Netz, and J. Beuthan, "Near-infrared diffuse optical tomography," *Dis. Markers*, vol. 18, pp. 313–337, 2002.